Vacuum 108 (2014) 39–44

Contents lists available at ScienceDirect

Vacuum

journal homepage: www.elsevier.com/locate/vacuum

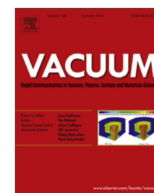

Free-carrier absorption and Burstein–Moss shift effect on quantum efficiency in heterojunction silicon solar cells

Sangho Kim [a], Jinjoo Park [b], Sunbo Kim [a], Youngseok Lee [a], Shihyun Ahn [b], Jaehyun Cho [b], Minkyu Ju [b], Nariangadu Lakshminarayan [c], Vinh Ai Dao [b,*], Junsin Yi [a,b,*]

[a] Department of Energy Science, Sungkyunkwan University, Suwon 440-746, South Korea
[b] College of Information and Communication Engineering, Sungkyunkwan University, Suwon 440-746, South Korea
[c] Department of Physics, Madras Christian College, Chennai 600059, India

ARTICLE INFO

Article history:
Received 27 December 2013
Received in revised form
21 May 2014
Accepted 21 May 2014
Available online 2 June 2014

Keywords:
Burstein–Moss effect
Free-carrier absorption
Spectroscopic ellipsometry
Heterojunction solar cells

ABSTRACT

Effects of the carrier concentration on the dielectric function of indium tin oxide (ITO) films were investigated by spectroscopic ellipsometry using Tauc–Lorentz and Drude oscillator terms. The real and imaginary parts of dielectric function values increased with increasing carrier concentration. Samples with lower refractive indices had (440) preferable crystallographic orientations. A more significant Burstein–Moss (B–M) effect leads to a lower extinction coefficient ($\boldsymbol{k}$) value in the short-wavelength regions, while more Free-carrier absorption (FCA) leads to a higher $\boldsymbol{k}$ value in the near-infrared region. The electrical properties obtained from optical studies, such as the carrier concentration and the carrier mobility, were compared with those obtained by van der Pauw measurements. The observed discrepancies between optically and electrically obtained values were due to carrier transport and grain boundaries. ITO films with a widened band gap energy due to the B–M shift are key to improve quantum efficiency (QE) at short-wavelengths in heterojunction silicon (HJ) solar cells. The reduced QE at long-wavelengths is attributed to optical scattering in the ITO films due to FCA. Despite widening the band gap, the short-circuit current density (J_{sc}) decreased from 36.27 mA/cm^2 to 34.17 mA/cm^2 with increasing carrier concentration from 6.15 × 10^{20} cm^{-3} to 9.84 × 10^{20} cm^{-3}. This result demonstrates that the FCA effect may affect J_{sc} more in HJ solar cells. The ITO film, prepared at the lowest carrier concentration, was used as an antireflection layer to fabricate HJ solar cells via optimization of the passivated layer. It resulted in a cell efficiency of 19.12% and an open-circuit voltage of 702 mV.

© 2014 Elsevier Ltd. All rights reserved.

1. Introduction

With their unique functional properties, indium tin oxide (ITO) films have been extensively studied and used in electronic and optoelectronic devices, such as organic light-emitting diodes [1], liquid-crystal displays [2], plasma-panel displays [3], thin-film (amorphous and microcrystalline) silicon solar cells [4], and conventional silicon solar cells with shallow emitters [5]. However, ITO films may not be adapted for use in conventional silicon solar cells due to shortcoming, such as free-carrier absorption (FCA) in the near-infrared region, degradation at high-process temperature, and the lack of surface passivation properties. In heterojunction silicon (HJ) solar cells, to obtain high efficiency, a key factor is to reduce optical loss. This optical loss can be reduced by (i) an optimized textured surface and (ii) use of a high-quality transparent conductive oxide with low FCA [6].

Thus, the ITO films that are used as antireflection electrodes in HJ solar cells have to be manufactured so that they show maximum conductivity as well as optical transparency over the entire wavelength region. High conductivity can be achieved by increasing the carrier concentration and also Hall mobility. When the carrier concentration in ITO films exceeds the Mott critical density value of 10^{18} to 10^{19} cm^{-3} [7], the films undergo a semiconductor-to-metal transition. This transition leads to optical losses in the near-infrared region due to FCA within the films, which, in turn, reduces the transparency in the near-infrared region [6]. With increases in carrier concentration, on the other hand, the band gap energy of ITO films can be increased because of the Burstein–Moss (B–M)

* Corresponding authors. College of Information and Communication Engineering, Sungkyunkwan University, Suwon 440-746, South Korea. Tel.: +82 31 290 7139; fax: +82 31 290 7179.
E-mail addresses: daovinhai@skku.edu (V.A. Dao), yi@yurim.skku.ac.kr (J. Yi).

http://dx.doi.org/10.1016/j.vacuum.2014.05.015
0042-207X/© 2014 Elsevier Ltd. All rights reserved.

effect, which enhances the light transparency within ITO films, in the short-wavelength region [6]. Thus, to provide a film that can satisfy the requirements of low carrier concentration, high energy band gaps, and high conductivity simultaneously and thus provide the highest quantum efficiency for HJ solar cells, the carrier concentration relative to the band gap energy of ITO films should be optimized carefully.

Using computer simulation, with the Drude model, electrical properties, such as the carrier concentration and the carrier mobility, can be determined using the position of the plasma edge (λ_p) and the damping of Drude oscillation (Γ_D) [8]. Using reflectance/transmittance data and Drude's theory, Dao et al. determined the electrical properties for aluminum-doped zinc oxide thin-films [9]. A similar procedure was used by Mergel et al. [8]. They reported that the electrical properties, determined optically from the reflectance/transmittance data, seemed higher than those estimated by van der Pauw measurements. Electrical properties can also be obtained using the spectroscopic ellipsometry (SE) technique combined with Drude theory, as shown by Fujiwara et al. [10]. However, in that report, the electrical properties were a little lower than those estimated by the van der Pauw method. Recently, Fachun Lai et al. used the Forouhi-Bloomer model, together with the modified Drude model, to determine electrical properties [11]. Consistent with Mergel et al., Fachun Lai et al. confirmed that the values of the carrier concentration determined optically were higher than those estimated by the van der Pauw method. However, the carrier mobility values determined by Fanchun Lai et al. were lower than those obtained by Mergel et al. Thus, in only a few studies has determining electrical properties of ITO films based on contactless techniques been attempted and they indicate a degree of uncertainty [8–11]. This was the issue that motivated the present study.

In this paper, the effects of carrier concentration on the dielectric function of ITO films using SE were assessed. Based on SE results, the optical carrier concentration (N_{opt}) and optical mobility (μ_{opt}) were obtained and compared with the corresponding values obtained from van der Pauw measurements. The effects of FCA and B–M shift in ITO films on the quantum efficiency and then the short-circuit current density (J_{sc}) of HJ solar cells were investigated in detail.

2. Experimental

ITO films were deposited from an ITO target containing 90 wt.% of In_2O_3 and 10 wt.% of SnO_2 by the radio frequency (rf) magnetron sputtering technique on commercially available polished Corning Eagle glass substrates. The substrates were cleaned thoroughly in acetone, isopropyl alcohol, and de-ionized water baths, in that order. The chamber of the sputtering unit was evacuated to a pressure of 1.33×10^{-3} Pa before admitting argon (99.999% purity) to maintain a pressure of 2.67×10^{-1} Pa. The carrier concentration of the ITO films was controlled by changing the rf-power from 0.27 to 1.10 W/cm^2. Before deposition, the target was treated with pre-sputtering for 10 min to normalize the initial sputtering condition of the target surface and during this time the substrates were not exposed to the target; with the aid of a shutter. The target-substrate distance was fixed at 2.6 cm to ensure that $\lambda_\mathbf{d}/d > 0.8$, where $\lambda_\mathbf{d}$ is the mean free path length of sputtered particles and d is the target-substrate spacing, so that the sputtered particles could reach the substrate with relatively high energies and there was a less possibility of scattering [12].

All the deposited films were characterized by spectroscopic ellipsometry (HR-190) at room temperature, in the energy range of 0.7–5.2 eV at an incidence angle of 75°. The dielectric functions of the films were analyzed using the Lorentz–Drude model. From this parametric modeling, we estimated the electrical properties of the films. The electrical properties of the ITO films were also obtained from Hall measurements in the van der Pauw geometry in dark conditions. The structures of the ITO films were determined by X-ray diffraction (XRD) profiles, using Bruker AXS D8 Discover and CuK$_\alpha$ radiation.

A Czochralski-grown Si wafer with thickness of 200 μm, and resistivity of ~1–10 Ω cm, was used to fabricate HJ solar cells. To reduce surface reflectance, the wafer was textured using de-ionized water, NaOH, and IPA solution for 30–34 min, followed by RCA 1 and RCA 2 cleaning and ultrasonic rinsing. Immediately before a-Si:H deposition, native oxide was removed from the wafer by dipping in 1% hydrofluoric acid for 1 min. Then, the a-Si:H (p/i) layers were deposited on the front surface of the silicon wafer at 200 °C by plasma-enhanced chemical vapor deposition. The ITO film was deposited using a metal mask that was directly placed on the a-Si:H surface to form square-shaped ITO layers. Then silver (Ag)/aluminum (Al) fingers were evaporated as front contacts. Finally, the a-Si:H (i/n) was deposited prior to the Al back contact deposition to create good ohmic contact. The structure of the fabricated solar cells in this study was Al/Ag/ITO/a-Si:H(p)/a-Si:H(i)/c-Si(n)/a-Si:H(i)/a-Si:H(n)/Al. Reactive ion etching was carried out using SF_6 gas on the top side for mesa-etching. The active area of the solar cell was 0.6×0.6 cm^2. The external quantum efficiency (QE) were measured using a xenon lamp, a monochromator, and optical filters, which filtered out the high orders with the light probe beam impinging normal to the samples. The relative QE of the samples were then calculated with respect to a calibrated reference cell. The solar cell performance was characterized by current–voltage measurements under Air Mass 1.5 Global (100 mW/cm^2, AM1.5G) at 25 °C conditions.

3. Results and discussion

Table 1 shows the Hall resistivity (ρ), Hall carrier concentration (N_{Hall}), and Hall mobility (μ_{Hall}) of the ITO films for different rf-power densities. The ρ values were found to decrease, from 3.39 to 1.15×10^{-4} Ω cm when the rf-power density was increased, from 0.27 to 1.10 W/cm^2. As a result, both N_{Hall} and μ_{Hall} increased, from 6.15 to 9.84×10^{20} cm^{-3} and 29.92–44.87 cm^2/Vs, respectively. When the rf-power was increased, sputtered-neutrals and sputtered-ions can reach the substrate surface with sufficient energy to start a crystalline growth phase [13]. The higher rf-power may also result in higher heat radiation from the target and

Table 1
Deposition conditions, N_{Hall}, μ_{Hall}, ρ, and film thickness are shown. The fit parameter of E_p was determined graphically from the photon energy position where $\boldsymbol{\varepsilon_1}(E) = 0$ and Γ_D was deduced from dielectric function modeling using the Drude model. The $\boldsymbol{\varepsilon_\infty}$ can be determined from the intercept at $1/(E^2 + \Gamma_D^2)$ in the plot of $\varepsilon_1(E)$ versus $1/(E^2 + \Gamma_D^2)$. The $[\boldsymbol{O_i}]$ can be calculated from XRD spectra [4]. The MSE, the sum of the squares of differences between each measured and experimental data point, is also indicated. The thickness for the surface roughness layer and the bulk layer are denoted as $\boldsymbol{d_s}$ and $\boldsymbol{d_b}$, respectively.

Sample no.	N_1	N_2	N_3	N_4
Power (W/cm^2)	0.27	0.55	0.82	1.10
N_{Hall} (10^{20} cm^{-3})	6.15	7.84	8.53	9.84
μ_{Hall} (cm^2 V^{-1} s^{-1})	29.92	38.85	43.96	44.87
ρ ($\times 10^{-4}$ Ω cm)	3.391	2.084	1.617	1.146
$[O_i]$ (10^{20} cm^{-3})	0.61	1.69	1.75	1.84
MSE	1.138	0.795	0.989	1.204
d_s (nm)	1.125 ± 0.235	1.783 ± 0.172	1.319 ± 0.222	1.209 ± 0.212
d_b (nm)	96.7 ± 0.153	93.4 ± 0.102	94.7 ± 0.137	96.3 ± 0.156
Γ_D (10^{-3} eV)	9.24 ± 0.0007	7.22 ± 0.0008	6.95 ± 0.0007	6.51 ± 0.0007
E_p (eV)	0.853	0.894	0.900	0.934
ε_∞ (eV)	3.9212	3.8945	3.8524	3.7293

Download English Version:

https://daneshyari.com/en/article/1689866

Download Persian Version:

https://daneshyari.com/article/1689866

Daneshyari.com